ACRS 2022
MONGOLIA

BACKSCATTERING AND INTERFEROMETRIC CHARACTERISTICS OF FLOOD DAMAGE IN KORIYAMA CITY CAUSED BY TYPHOON HAGIBIS

T. Igarashi [1] and H. Wakabayashi [2]

[1] Graduate School of Engineering, Nihon University, Japan – ceta21001@g.nihon-u.ac.jp
[2] College of Engineering, Nihon University, Japan – wakabayashi.hiroyuki@nihon-u.ac.jp

KEY WORDS: backscattering coefficient, interferometric coherence, gamma naught, principal component analysis

ABSTRACT:

Typhoon Hagibis hit Koriyama City in Fukushima prefecture, Japan, on October 13, 2019. The outflow of the rivers, such as Abukuma, Sasahara, Yata, and Ouse, caused flood damage to built-up areas in the city center. In addition, the flood caused damage to rice production because flooding in rice paddies happened just before harvest time. Our research objective is to clarify the Sentinel-1 backscattering and interferometric coherence change in inundated built-up areas and rice paddy fields in Koriyama City caused by Typhoon Hagibis. Backscattering and interferometric analyses were applied to Sentinel-1 data acquired before, during, and after flooding. The objective is to find the difference in backscattering coefficient and interferometric coherence in non-flood and flooded areas. The backscattering coefficient increases in the built-up area during flooding, which was significant in a residential area. The backscattering coefficient decreases in rice paddy fields. InSAR coherence decreases in built-up areas and rice paddy fields during flooding. However, the decrease in paddy fields was minimal. Also, the second component of principal component analysis (PCA) for multi-temporal backscattering images is potentially effective in detecting flooding simultaneously in built-up areas and rice paddy fields. For our future study, we want to apply a learning-based method to detect flooding in both built-up areas and rice paddy fields by using the results of this study.

1. INTRODUCTION

Typhoon Hagibis(No. 19, 2019 in Japan) landed in Japan on October 12, 2019. Many areas where the typhoon passed, such as Kanto, Koshin, and Tohoku regions, were heavily damaged by flooding. Especially in the southern part of the Tohoku region, a wide range of out-of-river flooding occurred in the Abukuma River basin, causing considerable flood damage in built-up areas. For example, in Koriyama City, Fukushima prefecture, the Abukuma River and its tributaries, such as the Sasahara, Yata, and Ouse Rivers, caused inundation above the floor in 6542 cases and inundation below the floor in 847 cases (Koriyama City, 2019). In addition, the flood caused damage to rice production because flooding in rice paddies happened just before harvest time in the Tohoku region.

Sentinel-1B acquired its data in the early morning of October 13 when the flood area reached its maximum, covering Koriyama City and its surroundings. Therefore, it would be suitable for analyzing the effect of inundation on the synthetic aperture radar (SAR) data. Although the initial analysis results have been reported(Wakabayashi et al., 2022), the further quantitative analysis should be necessary.

When the rice paddies' water depth reaches the top of the rice plant, the dominant backscattering mechanism of the smooth water surface becomes a specular reflection. Therefore, if a SAR observes the fully flooded rice paddy fields, it has lower backscattering coefficients than non-flood rice paddies. Many methods have been proposed for optimizing the backscatter threshold (Henry et al., 2006 and Martinis et al., 2009), such as the split-based automatic thresholding applied to TerraSAR-X data (Martinis et al., 2015), a combination of image segmentation and the surface scattering model applied to CosmoSkyMed X-band SAR data (Pulvirenti et al., 2011), and an automated Sentinel-1-based processing chain designed for flood detection and monitoring in near real-time (Twele et al., 2016).

When a flood occurs in built-up areas, such as urban or residential areas, it is well known that a double bounce scattering between the building wall and the water surface increases. However, since the change of backscattering coefficient is complicated depending on the azimuthal angle of the buildings and vegetation cover on the ground, the same thresholding method cannot apply to the built-up areas. An alternative method for detecting inundation areas is to use the coherence calculated by the interferometric SAR(InSAR) analysis. The coherence can recognize changes in the backscattering mechanism between two data acquisition intervals, and coherence decreases in flooded areas, even urban and vegetated areas (Refice et al., 2014, Pulvirenti et al., 2016, Chini et al., 2019, and Ohki et al., 2019).

In addition, there are examples of detecting a flood area by applying principal components analysis(PCA) to multi-temporal SAR images (Calabresi, 1995, and Henebry and Rieck, 1996), and texture information derived from the gray level co-occurrence matrix (GLCM) (Haralick et al., 1973) can also apply to detect flooded areas(Sohn et al.,2005 and Dasgupta et al.,2017).

This study aims to clarify the effect of flood damage on the Sentinel-1 data for the flood areas in both built-up areas and rice paddy fields in Koriyama City caused by Typhoon Hagibis. The backscattering and InSAR analyses were applied to both built-up areas and paddy fields to quantitatively understand the effect of flood damage on the backscattering coefficient and InSAR coherence.

2. TEST SITE AND SENTINEL-1 DATA

The urban area is located in the center of Koriyama City and is surrounded by agricultural areas. The Abukuma River runs through the center of the city from north to south, and the flood damage was concentrated around the Abukuma River in 2019.

Five districts with flood-damaged and four non-damaged areas were extracted in Koriyama City by referring to the inundation

area issued by Koriyama City (Koriyama City, 2019) and the aerial photographs taken by the Geospatial Information Authority of Japan(GSI) (GSI, 2019). Table 1 summarizes the nine extracted sites used in this study, and Figure 1 shows the locations of nine sites indicated on Sentinel-1 VV data acquired on October 13.

The analysed SAR data used were Interferometric Wide Swath(IW) mode data that Sentinel-1A and 1B observed at the test site in the morning on September 24, October 7, 13, 19, and 31, 2019. The IW mode employs the Terrain Observation with Progressive Scans SAR (TOPSAR) technique (Zan and Guarnieri, 2006) to acquire data over a 250-km swath with a spatial resolution of approximately 5 m (range) x 20 m (azimuth) on the slant range. The incidence angle ranges from 29 ° to 46 ° in the IW mode. The Koriyama city area locates at about a 35° of incidence angle.

Table 2 summarizes the list of InSAR datasets and observation times. Two images acquired on September 24 and October 7 have no effect of inundation found. The image on October 13 was acquired when the flooding expanded to the maximum area. The other two images on October 19 and 31 were acquired after the flooding had retreated.

Table 1 List of sample areas in Koriyama City

site no.	flood or non-flood	land cover	area (ha)	area name
1	flood	built-up area	234	Chuo-Kogyo-Danchi
2	flood	paddy field	52	East of Chuo-Kogyo-Danchi
3	flood	built-up area	133	Shokuhin-Danchi
4	flood	paddy field	25	North of Fukuyama-Clean-Center
5	flood	built-up area	31	Teikyo Asaka
6	non-flood	built-up area	38	West of Koriyama station
7	non-flood	paddy field	40	South of Nihon Univerisity
8	non-flood	built-up area	127	Asaka-machi
9	non-flood	paddy field	68	South of Asaka-machi

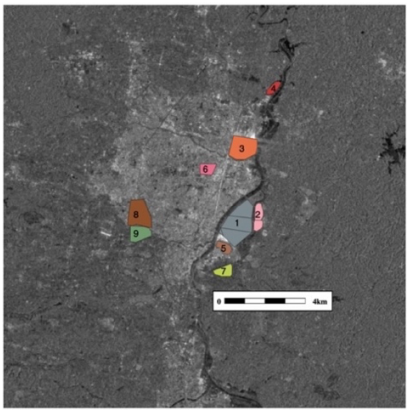

Figure 1 Location of nine sites (polygon) in Table 1 indicated on Sentinel-1 C-band SAR VV data acquired on Oct.13,2019.

Table 2 List of InSAR dataset

InSAR dataset	B_p (perpendicular baseline)	temporal baseline	Acquisition time(JST)
pair-1 Descending	-52.46m	12 days	・Sep.24 5:43(Sentinel-1A)
			・Oct. 7 5:43(Sentinel-1A)
pair-2 Descending	+14.20 m	6 days	・Oct. 7 5:43(Sentinel-1A)
			・Oct. 13 5:42(Sentinel-1B)
pair-3 Descending	-29.65 m	6 days	・Oct. 13 5:42(Sentinel-1B)
			・Oct. 19 5:43(Sentinel-1A)
pair-4 Descending	+63.74 m	12 days	・Oct. 19 5:43(Sentinel-1A)
			・Oct. 31 5:43(Sentinel-1A)

3. SENTINEL-1 DATA PRE-PROCESSING AND ANALYSIS

The European Space Agency (ESA) Copernicus Open Access Hub provided both Level-1 Ground Range Detected(GRD) and Slant Range Complex(SLC) data for the backscattering and InSAR analyses. The ESA also provided Sentinel Toolbox to pre-process the GRD and SLC data.

After fetching the high-precision orbital data, we applied the thermal noise removal and the radiometric calibration to gamma-naught(γ^0) with terrain flattening to the GRD data. The γ^0 was used instead of the backscattering coefficient (σ^0) to reduce the sensitivity to the effect of incidence angle. Finally, the data were projected onto the UTM coordinate (Zone 54) with a pixel spacing of 10 m. The Shuttle Radar Topography Mission (SRTM) Digital Elevation Model (DEM) with a 1-arc second (30 m) grid was applied in both radiometric terrain flattening and ortho-rectified processing.

We also applied the co-registration and deburst processing to the IW-2 sub-swath for the InSAR pre-processing. Then, the phase difference and coherence were estimated, followed by the geometric projection onto the UTM coordinate(Zone 54) with a pixel spacing of 10m. Figure 2 shows the RGB color-composite images using 3-days γ^0 and 3-sets of coherence images.

For extracting the backscattering coefficients and InSAR coherence of the nine sites given in Table 1, each area was clipped using the polygon of the nine sites, and the average and standard deviation in each site were calculated.

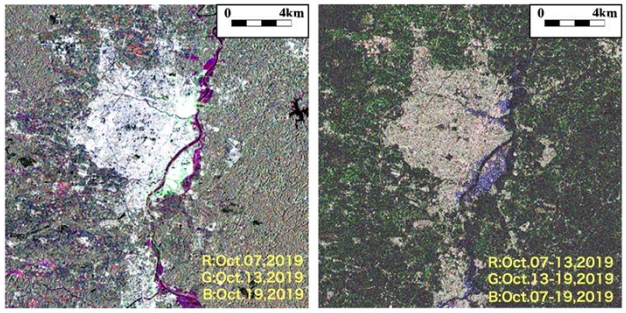

(a) (b)

Figure 2 Gamma-naught and coherence images covering Koriyama city area (a) RGB colored gamma-naught image, and (b)RGB colored coherence image.

4. RESULT AND DISCUSSION

When a flood occurs in the built-up area, specular reflection occurs on the water surface, and the double-bounce scattering component of the building wall and water surface increases. As a result, the backscattering coefficient increases. When a full flood occurs at rice paddy fields during the rice-growing season, the specular reflection from the water surface becomes dominant, and then the backscattering coefficient decreases. Figure 3 (a) and 3 (b) show changes in γ^0 in the built-up areas and paddy fields. The difference between flood-damaged areas(Area 1-5) and non-flood areas(Area 6-9) was evident.

The coherence decreases when one of the InSAR data pairs is taken in a flood situation because the scattering mechanism changes between InSAR data pairs in both built-up and rice paddy areas. Figure 4 (a) and 4 (b) show the coherence changes in the built-up area and the rice paddy field. The coherence

decreased when one of the InSAR data pairs was inundated in both cases. However, since the coherence in the paddy field area is as small as 0.3, even in the non-flooded area, it is difficult to detect the inundation-damaged paddy fields only by interferometric coherence.

Considering the effects on γ^0 images with inundated, we attempted to detect flooded areas simultaneously in built-up and paddy fields. Figure 5 shows the second principal component calculated from multi-temporal γ^0 images on October 7, 13, and 19. When the PCA is applied to the multi-temporal γ^0 image, the first principal component shows a synthesized variable that maximizes the variance of the unchanged areas in the multi-temporal γ^0 image. The second component is a synthesized variable orthogonal to the first principal component and is considered to emphasize the changing region of the multi-temporal γ^0 image. In Figure 5, we can recognize the bright area as a flooded built-up area and the dark areas as a flooded paddy.

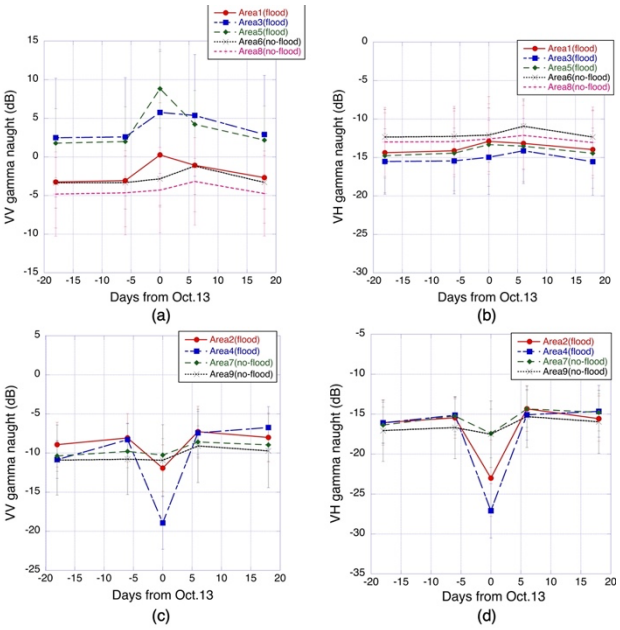

Figure 3 Change of gamma-naught.
(a)VV change in built-up area, (b)VH change in built-up area, (c)VV change in paddy field, and (d)VH change in paddy field.

5. SUMMARY

In order to clarify the characteristics of the flood-damaged area appearing in the backscattering coefficient and InSAR coherence, we analysed the Sentinel-1data at the area damaged by typhoon Hagibis Koriyama City, Fukushima, Japan. The main results were given as follows,

(1) The backscattering coefficient(gamma-naught) increases in the built-up area during flooding, and the increase was significant in residential areas and small in industrial areas. On the other hand, the backscattering coefficient decreased during the flood period in paddy fields.
(2) InSAR coherence decreases in built-up areas and paddy fields with flood damage. However, the decrease in paddy fields is slight due to non-flood paddies having lower coherence than built-up areas.
(3) The second component of PCA analysis for multi-temporal backscattering images is potentially effective in simultaneously detecting flood damages in built-up areas and paddy fields.

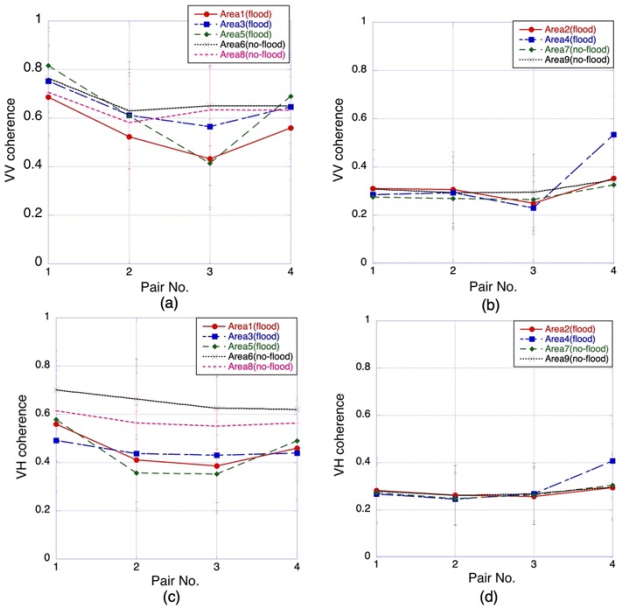

Figure 4 Change of InSAR coherence.
(a) VV coherence in built-up areas,(b) VV coherence in paddy fields, (c) VH coherence in built-up areas, and (d) VH coherence in paddy fields,

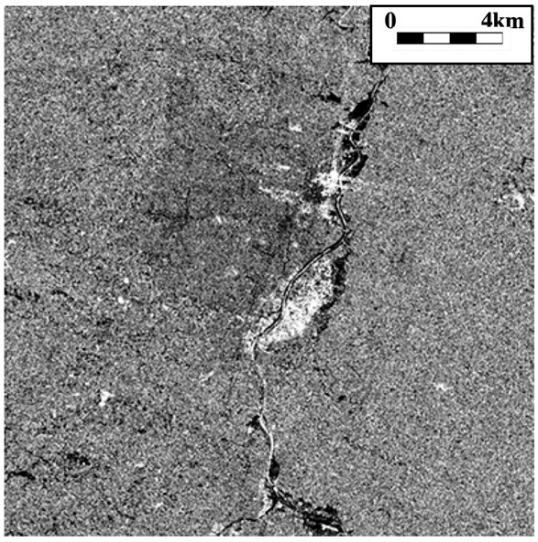

Figure 5 Result of PCA analysis applied to multi-temporal backscattering images (2nd. component)

Our further study includes texture analysis in addition to backscattering and InSAR coherence. We also want to apply a learning-based method to detect the flooded area in both built-up and paddy fields.

ACKNOWLEDGEMENTS

The ESA provided the Sentinel-1 SAR data used in this study.

REFERENCES

Damage of Typhoon No. 19 in Koriyama City: http://www.kageken.jp/2019_kageken/wp-content/uploads/2019/11/e22725bbd38ced8fb14d24d7e994e452.png (accessed on 12 September 2022)

Wakabayashi, H., Igarashi, T., and Tsukamoto, S. 2022, Flood damage analysis in Koriyama city caused by typhoon Hagibis using Sentinel-1 SAR data, Proceedings of International Geoscience and Remote Sensing Symposium, pp.6021-6024.

Henry, J. B., Chastanet,P., Fellah, K. and Desnos, Y. L., 2006. Envisat multi-polarized ASAR data for flood mapping, International Journal of Remote Sensing, Vol. 27, No. 10, pp. 1921–1929.

Martinis, S., Twele, A. and Voigt, S.,2009. Towards operational near real-time flood detection using a split-based automatic thresholding procedure on high resolution TerraSAR-X data, Natural Hazards Earth Syst. Sci., Vol. 9, No. 2, pp. 303–314.

Martinis, S., Kersten, J., and Twele, A.,2015. A fully automated TerraSAR-X based flood service," ISPRS J. Photogramm. Remote Sens., vol. 104, pp. 203–212.

Pulvirenti, L., Chini, M., Pierdicci, N., Guerriero, L., and Ferrazzoli, P., 2011. Flood monitoring using multi-temporal COSMO-SkyMed data: Image segmentation and signature interpretation," Remote Sens. Environ., vol. 115, no. 4, pp. 990–1002.

Twele, A., Cao, W., Plank, S., and Martinis, S., 2016. Sentinel-1- based flood mapping: a fully automated processing chain, International Journal of Remote Sensing, Vol. 37, No.13, pp. 2990-3004.

Refice, A. et al., 2014. SAR and InSAR for flood monitoring: Examples with COSMO-SkyMed data, IEEE J. Sel. Topics Appl. Earth Observ. Remote Sens., vol. 7, no. 7, pp. 2711–2722.

Pulvirenti, L., Chini, M., Pierdicca, N., and Boni, G., 2016. Use of SAR data for detecting floodwater in urban and agricultural areas: The role of the interferometric coherence, IEEE Trans. Geosci. Remote Sens., vol. 54, no. 3, pp. 1532–1544.

Chini, M., Pelich, R., Pulvirenti, L., Pierdicca, N., Hostache, R., and Matgen, P.,2019. Sentinel-1 InSAR coherence to detect floodwater in urban areas: Houston and hurricane Harvey as a test case," Remote Sens., vol. 11, p. 107.

Ohki, M. et al., 2019. Flood area detection using PALSAR-2 amplitude and coherence data: The case of the 2015 heavy rainfall in Japan, IEEE J. Sel. Topics Appl. Earth Observ. Remote Sens., vol. 12, no. 7, pp. 2288–2298.

Calabresi, G., 1995. The use of ERS data for flood monitoring: an overall assessment, Proceedings of the 2nd ERS Applications Workshop, pp. 237–241.

Henebry, G. M., and Rieck, D. R., 1996. Applying principal components analysis to image time series: effects on scene segmentation and spatial structure, Proceedings of International Geoscience and Remote Sensing Symposium, pp. 448-450.

Haralick, R. M., Shanmugam, K., and Dinstein, I., 1973. Textural Features for Image Classification," IEEE Trans. on Systems, Man and Cybernetics, Vol. 3, No. 6, pp. 610-621.

Sohn, H., Song, Y., and Kim, G., 2005. Detecting water area during flood event from SAR image," Lecture Notes in Computer Science, 3481, pp.771-780.

Dasgupta, A., Grimaldi, S., Ramsankaran, R., and Walker, J., 2017. Optimized glcm-based texture features for improved SAR-based flood mapping," Proc. of IEEE International Geoscience and Remote Sensing Symposium, pp.3258-3261.

Hazard map in Koriyama City:
https://www.city.koriyama.lg.jp/uploaded/attachment/36867.pdf
(accessed on 12 September 2022)

Information on Typhoon Hagiwara in the first year of Typhoon Hagibis by Geospatial Information Authority of Japan :
https://maps.gsi.go.jp/#10/37.397437/140.394974/&base=std&ls=std%7C20191012typhoon19_abukuma_1013naname&disp=11&lcd=20191012typhoon19_abukuma_1013naname&vs=c1j0h0k0l0u0t0z0r0s0m0f1&d=m
(accessed on 12 September 2022)

Zan, F. De and Guarnieri A. M. 2006, TOPSAR: Terrain observation by progressive scans. IEEE Trans. on Geoscience and Remote Sensing, Vol. 44, No. 9, pp. 2352-2360.